

ARTICLES

An inhibitor of NEDD8-activating enzyme as a new approach to treat cancer

Teresa A. Soucy¹, Peter G. Smith¹, Michael A. Milhollen¹, Allison J. Berger¹, James M. Gavin¹, Sharmila Adhikari¹, James E. Brownell¹, Kristine E. Burke¹, David P. Cardin¹, Stephen Critchley¹, Courtney A. Cullis¹, Amanda Doucette¹, James J. Garnsey¹, Jeffrey L. Gaulin¹, Rachel E. Gershman¹, Anna R. Lublinsky¹, Alice McDonald¹, Hirotake Mizutani¹, Usha Narayanan¹, Edward J. Olhava¹, Stephane Peluso¹, Mansoureh Rezaei¹, Michael D. Sintchak¹, Tina Talreja¹, Michael P. Thomas¹, Tary Traore¹, Stepan Vyskocil¹, Gabriel S. Weatherhead¹, Jie Yu¹, Julie Zhang¹, Lawrence R. Dick¹, Christopher F. Claiborne¹, Mark Rolfe¹, Joseph B. Bolen¹ & Steven P. Langston¹

The clinical development of an inhibitor of cellular proteasome function suggests that compounds targeting other components of the ubiquitin–proteasome system might prove useful for the treatment of human malignancies. NEDD8-activating enzyme (NAE) is an essential component of the NEDD8 conjugation pathway that controls the activity of the cullin-RING subtype of ubiquitin ligases, thereby regulating the turnover of a subset of proteins upstream of the proteasome. Substrates of cullin-RING ligases have important roles in cellular processes associated with cancer cell growth and survival pathways. Here we describe MLN4924, a potent and selective inhibitor of NAE. MLN4924 disrupts cullin-RING ligase-mediated protein turnover leading to apoptotic death in human tumour cells by a new mechanism of action, the deregulation of S-phase DNA synthesis. MLN4924 suppressed the growth of human tumour xenografts in mice at compound exposures that were well tolerated. Our data suggest that NAE inhibitors may hold promise for the treatment of cancer.

The ubiquitin–proteasome system (UPS) is responsible for the regulated degradation of intracellular proteins with important roles in a broad array of cellular functions¹. One drug which targets the UPS, the proteasome inhibitor bortezomib (Velcade), is approved for the treatment of patients with multiple myeloma or mantle cell lymphoma^{2,3}. The anti-cancer activity of bortezomib suggests that inhibitors of other enzymes that modulate UPS activity might lead to the development of new anti-cancer drugs with differentiated clinical use⁴.

Covalent linkage of the small protein modifier ubiquitin to a protein frequently acts to initiate a process that results in the degradation of the protein by the proteasome⁵. The ubiquitylation pathway is executed by a series of three distinct enzymatic steps. Ubiquitin is first ‘activated’ by ubiquitin-activating enzyme (E1) in an ATP-dependent reaction⁶. In the second step, ubiquitin is transferred from the E1 to an ubiquitin-conjugating enzyme (E2). The E2 then collaborates with a ubiquitin ligase enzyme (E3) to conjugate the ubiquitin to the substrate protein targeted for degradation.

Although the ubiquitylation pathway was the first such pathway to be discovered⁷, homologous pathways for protein conjugation by ubiquitin-like proteins (UBLs) have subsequently been identified⁸. One such conjugation pathway uses the ubiquitin-like protein NEDD8 (ref. 9). Similar to ubiquitin, NEDD8 is first activated by an E1 enzyme (NEDD8 activating enzyme (NAE; a heterodimer of NAE1 and UBA3 subunits)), transferred to an E2 enzyme (Ubc12, also known as UBE2M), and then conjugated to target substrates. The best characterized substrates of the NEDD8 pathway are the cullin family of proteins¹⁰. Cullin proteins function as a core scaffold for a subclass of ubiquitin E3 ligases, the cullin-RING ligases (CRLs)¹¹, and covalent modification of the cullin protein within the CRL by NEDD8 is required for holoenzyme ubiquitin ligase

activity^{12–14}. Recent work suggests that there are several mechanisms by which NEDD8 modification activates CRLs^{15,16}. Thus, one function of the NEDD8 pathway is to regulate the ubiquitylation rate (and degradation kinetics) of the subset of proteins whose ubiquitylation is dependent on CRLs.

Here we report the discovery of MLN4924, a small molecule inhibitor of NAE that is at present being evaluated in several phase I clinical trials. MLN4924 selectively inhibits NAE activity compared to the closely related ubiquitin-activating enzyme (UAE, also known as UBA1) and SUMO-activating enzyme (SAE; a heterodimer of SAE1 and UBA2 subunits), in purified enzyme and cellular assays. MLN4924 exhibits potent *in vitro* cytotoxic activity against a variety of human tumour-derived cell lines. Treatment of tumour cells with MLN4924 increases the abundance of known CRL substrates, but unlike proteasome inhibition by bortezomib, MLN4924 did not significantly inhibit bulk protein turnover. In the human cell lines studied, the mechanism of cell death seems to be a consequence of uncontrolled DNA synthesis in the S-phase of the cell cycle leading to DNA damage and induction of apoptosis. *In vivo*, MLN4924 demonstrates potent anti-tumour activity in mice bearing human tumour xenografts, at drug exposures that are well tolerated.

MLN4924 is a selective inhibitor of NAE

MLN4924 was discovered as a result of iterative medicinal chemistry efforts on N6-benzyl adenosine that was originally identified as an inhibitor of NAE via high throughput screening (see Supplementary Information for chemical characterization). As shown in Fig. 1a, MLN4924 is structurally related to adenosine 5′-monophosphate (AMP)—a tight binding product of the NAE reaction^{6,17}. The main differences between AMP and MLN4924 are: (1) in place of the adenine base, MLN4924 has a deazapurine base substituted with an

¹Discovery, Millennium Pharmaceuticals, Inc., 40 Landsdowne Street, Cambridge, Massachusetts 02139, USA.

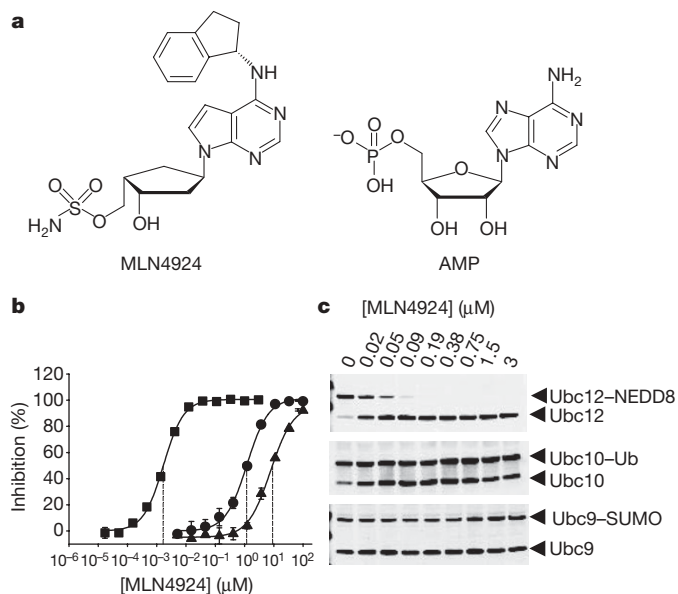


Figure 1 | MLN4924 is a potent and selective inhibitor of NEDD8-activating enzyme. **a**, Chemical structure of MLN4924 ((1*S*,2*S*,4*R*)-4-[(1*S*)-2,3-dihydro-1*H*-inden-1-ylamino]-7*H*-pyrrolo[2,3-*d*]pyrimidin-7-yl]-2-hydroxycyclopentyl)methyl sulphamate. The structure of AMP is shown for comparison. **b**, MLN4924 demonstrates potent and selective inhibition of NAE (squares) *in vitro* ($\text{IC}_{50} = 4.7 \pm 1.5 \text{ nM}$) compared to SAE (triangles) and UAE (circles) (IC_{50} values of $8.2 \pm 6.2 \mu\text{M}$ and $1.5 \pm 0.71 \mu\text{M}$, respectively). **c**, MLN4924 selectively inhibits NAE in cells. Inhibition of NAE, SAE and UAE in cells was assessed by immunoblot analysis of the Ubc12-NEDD8, Ubc9 (also known as UBE2I)-SUMO and Ubc10-Ub thioester levels respectively, in HCT-116 cell lysates.

aminoindane at N6; (2) in place of the ribose sugar, MLN4924 has a carbocycle and the equivalent of the 2'-hydroxyl group of AMP is absent; (3) in place of the phosphate, MLN4924 has a sulphamate; and (4) in contrast to the stereochemistry of AMP, the methylene sulphamate of MLN4924 is in a non-natural anti-relationship to the deazapurine. X-ray crystallography confirmed that MLN4924 bound in the nucleotide-binding site of NAE^{18,19} (J.E.B. *et al.*, manuscript in preparation).

MLN4924 is a potent inhibitor of NAE (half-maximal inhibitory concentration (IC_{50}) = $0.004 \mu\text{M}$), and is selective relative to the closely related enzymes UAE, SAE, UBA6 and ATG7 (IC_{50} = 1.5, 8.2, 1.8 and $>10 \mu\text{M}$, respectively) when evaluated in purified enzyme assays that monitor the formation of E2-UBL thioester reaction products (Fig. 1b and data not shown). The selectivity profile of MLN4924 for NAE was also evident in cell-based assays evaluating the levels of E2-UBL thioester products by immunoblotting (Fig. 1c). Molecules of this general class have been shown to inhibit transfer RNA synthetases²⁰. To rule out this possibility, MLN4924 was shown to have no effect in an assay monitoring the incorporation of [³⁵S]methionine into newly synthesized proteins (Supplementary Fig. 1). Furthermore, MLN4924 did not demonstrate detectable inhibition of other ATP-using enzymes (Supplementary Table 1).

NAE regulates a subset of UPS substrates

Polyubiquitinated proteins are normally degraded by cellular proteasomes, and inhibition of proteasome activity has been shown to substantially suppress bulk intracellular protein turnover²¹. In contrast, inhibition of the NAE pathway should only affect the degradation of proteins whose ubiquitinylation is mediated by CRLs. The effect of NAE inhibition on total intracellular protein turnover and proteasome-dependent protein turnover was examined by comparing the consequence of NAE inhibition and proteasome inhibition on the degradation of metabolically labelled proteins in cultured HCT-116 cells. MLN4924 and bortezomib were used at concentrations that

result in rapid and complete inhibition of detectable CRL and proteasome activity, respectively (Supplementary Fig. 2). As early as 15 min after treatment, bortezomib was found to inhibit protein turnover, whereas MLN4924 did not have a significant effect (Fig. 2, inset). Over longer exposure times, MLN4924 treatment inhibited overall protein turnover by $\approx 9\%$ ($P = 0.023$), and bortezomib treatment inhibited protein turnover by $\approx 50\%$ ($P < 0.001$) as estimated from the associated area under curve (AUC) values from 2–4 h. These observations suggest that in HCT-116 cells, approximately 20% of the proteasome-dependent degradation is mediated by CRL-ubiquitinylation.

NAE inhibition results in S-phase defects

NAE inhibition and subsequent decrease in the steady-state level of Ubc12-NEDD8 thioesters in cells treated with MLN4924 predicts that a corresponding decrease in the abundance of NEDD8-cullin conjugates should be observed. Moreover, inhibition of this pathway should also result in the diminished activity of CRLs leading to the accumulation of CRL-target proteins. Treatment of HCT-116 cells with MLN4924 for 24 h resulted in a dose-dependent decrease of Ubc12-NEDD8 thioester and NEDD8-cullin conjugates, with an $\text{IC}_{50} < 0.1 \mu\text{M}$ (Fig. 3a), resulting in a reciprocal increase in the abundance of the known CRL substrates CDT1 (refs 22–24), p27 (refs 14, 25) and NRF2 (also known as NFE2L2)²⁶, but not non-CRL substrates (Supplementary Fig. 3). In similar experiments, we have observed the accumulation of other CRL substrates including c-Jun²⁷, HIF1 α (ref. 28), cyclin E²⁹, CDC25A (ref. 30), EMI1 (also known as FBXO5)³¹ and phosphorylated I κ B α (refs 13, 32) (data not shown).

The observed accumulation of CRL substrates in MLN4924-treated HCT-116 cells is consistent with the idea that the abundance of most, if not all, CRL target proteins can be modulated by NAE inhibition. However, the cellular consequences of such inhibition could conceivably vary depending on numerous physiological parameters regulated by proteins under the control of different CRLs in different cell types. In HCT-116 cells, the most prominent phenotype observed was the disruption of S-phase regulation leading to cellular death (Fig. 3b).

In these experiments, HCT-116 cells were treated with $0.3 \mu\text{M}$ MLN4924, a concentration sufficient to decrease the steady-state level of NEDD8-cullin conjugates by $>80\%$ relative to untreated cells

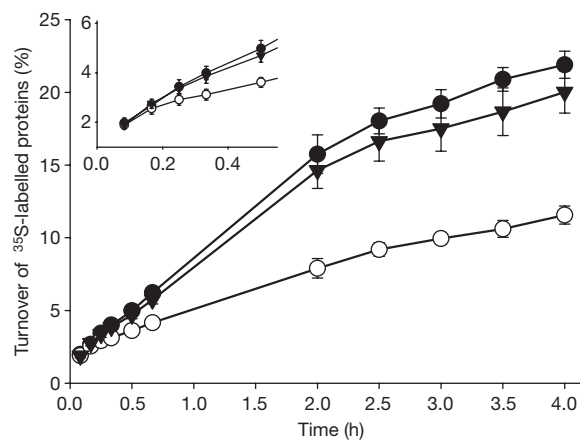


Figure 2 | NEDD8 pathway inhibition, in contrast to proteasome inhibition, minimally affects bulk intracellular protein turnover. The proteins in HCT-116 cells were metabolically labelled by culturing the cells for 20 min in the presence of [³⁵S]methionine. The cells were then chased with fresh media containing excess cold methionine and dimethylsulphoxide (DMSO) (filled circles), $3 \mu\text{M}$ MLN4924 (filled triangles) or $3 \mu\text{M}$ bortezomib (open circles). Protein degradation, measured by the appearance of radioactivity in the media over time, was determined as described in Methods. Inset, expanded view of early timepoints. Error bars show s.d.; $n = 6$.

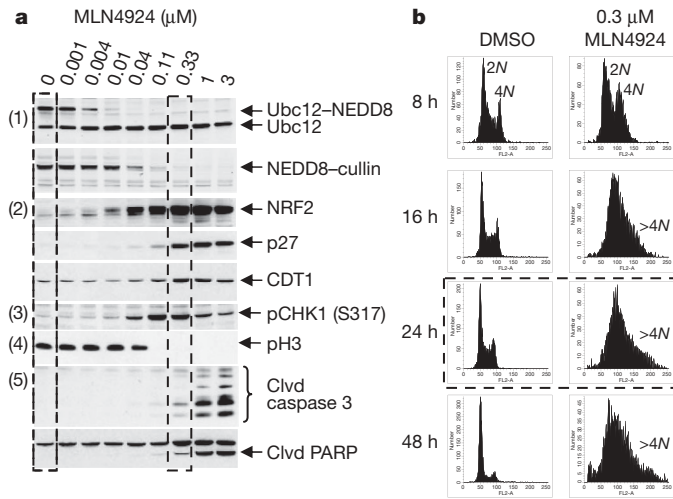


Figure 3 | Inhibition of the NEDD8 pathway in cells results in S-phase defects, DNA damage and apoptosis. **a**, HCT-116 cells were treated with MLN4924 for 24 h. Cell lysates were immunoblotted for (1) Ubc12–NEDD8 and NEDD8–cullin conjugate levels, (2) CRL substrates, NRF2, p27 and CDT1, (3) DNA damage marker, phosphorylated CHK1 (Ser 317), (4) mitotic marker pH3, and (5) apoptotic markers, cleaved (Clvd) caspase 3 and cleaved PARP. **b**, HCT-116 cells were treated with DMSO or 0.3 μM MLN4924 for 8, 16, 24 and 48 h. DNA profiles were analysed by flow cytometry. $>4N$ represents cells having greater than tetraploid DNA content.

(Fig. 3a, dashed outline), and the cell-cycle profiles were monitored by DNA content using flow cytometry. As early as 8 h after compound treatment, cells began to accumulate in S-phase (Fig. 3b). By 24 h, a significant fraction of cells contained $\geq 4N$ DNA content (Fig. 3b, dashed outline); however, the absence of detectable phosphohistone H3 (pH3) staining indicated that the cells were not transitioning into mitosis (Fig. 3a). By 48 h, an increase in the sub- $2N$ DNA content population was observed, consistent with cells undergoing apoptosis and further supported by the accumulation of cleaved caspase 3 and PARP (Fig. 3a).

The cell-cycle phenotype observed after MLN4924 treatment is similar to that of cells undergoing re-replication, a phenomenon in which several rounds of DNA synthesis are initiated in the absence of cycle progression. Although several mechanistic defects can result in such a phenotype, our finding that CDT1, a protein essential for 'licensing' origins of DNA replication^{33,34}, accumulated in MLN4924-treated cells (Fig. 3a) suggests that this substrate for CRL1^{SKP2} (refs 22–23, 35) and CRL4–DDB1^{CDT2} (refs 24, 36, 37) might represent an important mediator of MLN4924 activity. Forced expression of CDT1 in cells, or RNA interference (RNAi)-mediated ablation of the endogenous CDT1-inhibitor geminin, results in the DNA re-replication phenotype^{38–41}.

Re-replication is known to induce DNA damage and elicit cellular DNA damage signalling^{42,43}. We observed a MLN4924 concentration-dependent accumulation of phosphorylated CHK1 (at Ser 317; also known as CHEK1), indicative of DNA damage signal transduction through the ATM/ATR pathway⁴⁴. The levels of other DNA damage markers also increased in a similar manner (data not shown). Whether DNA damage signalling represents the primary event leading to the activation of apoptosis, or whether other alterations induced by inhibition of the NAE pathway can independently lead to cellular death will require further experimentation.

The observed phenotype is probably the result of specific effects of NAE inhibition by MLN4924, because ablation of NAE expression by short interfering RNA (siRNA) resulted in similar S-phase defects (Supplementary Fig. 4). Importantly, although NAE and proteasome inhibition induce apoptosis, the treatment of HCT-116 cells with proteasome inhibitors did not elicit re-replication or DNA damage

(data not shown). MLN4924 treatment of other human-tumour-derived cell lines, including Calu-6 (lung), SKOV-3 (ovarian), H460 (lung), DLD-1 (colon), CWR22 (prostate) and OCI-LY19 (lymphoma), also resulted in S-phase-defective phenotypes (data not shown). Different cells however, show variable sensitivity to the effects of MLN4924 treatment (Supplementary Table 2). The mechanism(s) underlying these differential sensitivities remains to be determined. Notably, the non-transformed MCF10A breast epithelial cells were more sensitive to MLN4924 when actively proliferating, consistent with the idea that cycling cells are more susceptible to NAE-inhibition-induced re-replication.

MLN4924 inhibits the NAE pathway *in vivo*

To assess the ability of MLN4924 to inhibit NAE *in vivo*, HCT-116 tumour-bearing mice received a single subcutaneous dose of 10, 30 or 60 mg kg^{-1} MLN4924, and tumours were excised at various time-points over the subsequent 24 h period. The pharmacodynamic effects of treatment were assessed in tumour lysates which were analysed for NEDD8–cullin, NRF2 and CDT1 protein levels (Fig. 4a–c). A single dose of MLN4924 resulted in a dose- and time-dependent decrease of NEDD8–cullin levels as early as 30 min after administration of compound (Fig. 4a), with maximal effect 1–2 h post-dose. A significant difference was observed between the 10 and 60 mg kg^{-1} response profiles ($P < 0.01$), although the 10 and 30 mg kg^{-1} ($P = 0.11$) and 30 and 60 mg kg^{-1} ($P = 0.24$) profiles were not significantly different from each other. A single dose of MLN4924 also led to a dose- and time-dependent increase in the steady state levels of NRF2 and CDT1 (Fig. 4b, c). For all dose levels, NRF2 protein levels peaked 2–4 h after administration of MLN4924 and started to decline by 4–8 h post-dose. The timing of CDT1 accumulation was slightly delayed compared to NRF2, peaking 4 h after MLN4924 administration (Fig. 4c). Evidence of DNA damage in the tumour was indicated by the increased levels of phosphorylated CHK1 (Ser 317) at 8 h after a single administration of 30 and 60 mg kg^{-1} MLN4924 (Fig. 4d). It should be noted that MLN4924 also decreased NEDD8–cullin levels in normal mouse tissue as illustrated in mouse bone marrow cells (Supplementary Fig. 5). These data suggest that MLN4924-mediated inhibition of

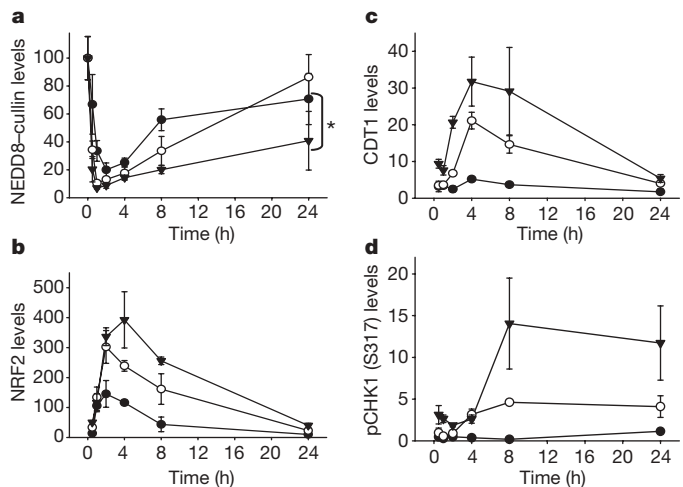


Figure 4 | MLN4924 inhibits the NEDD8 pathway resulting in DNA damage in human tumour xenografts. Mice bearing HCT-116 xenografts were administered a single subcutaneous dose of vehicle or MLN4924 at 10 mg kg^{-1} (filled circles), 30 mg kg^{-1} (open circles) or 60 mg kg^{-1} (filled triangles). Tumours were excised at the indicated times and NEDD8–cullin conjugate levels (**a**) and relative NRF2 protein levels (**b**) were measured in the tumour lysates (20 μg protein per lane) by quantitative immunoblot analysis. Units are arbitrary. **c**, **d**, CDT1 (**c**) and phosphorylated CHK1 (Ser 317) (**d**) levels were assessed by immunohistochemistry. Data are expressed as the percentage area of DAB stain. Error bars show s.d. $n = 3$; $*P < 0.01$.

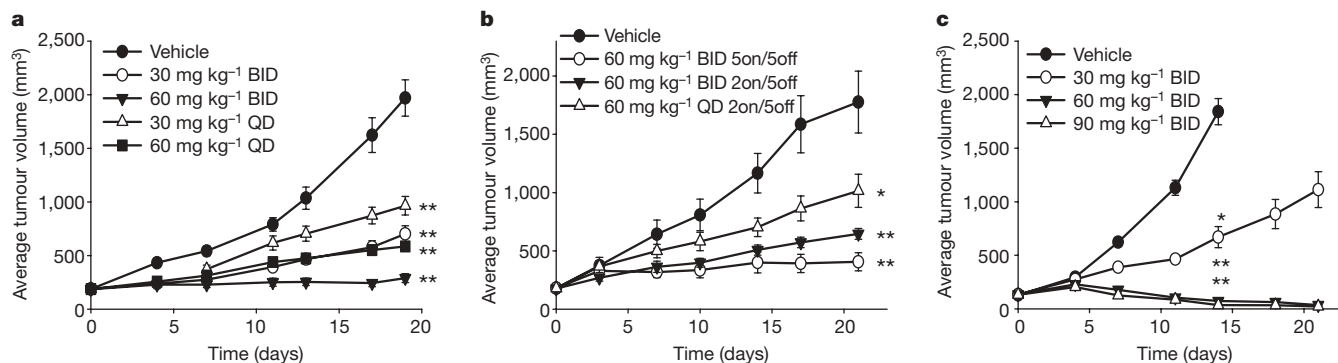


Figure 5 | MLN4924 produces tumour growth inhibition in human tumour xenografts. **a–c**, Nude mice bearing HCT-116 (**a**, **b**) or H522 (**c**) tumour xenografts were dosed by subcutaneous administration with either vehicle control or MLN4924 at the doses and schedules indicated. For example, 5on/

5off represents five days treatment followed by five days free of treatment, repeated for two cycles during the 21-day study. Mean tumour volumes \pm s.e.m. are shown. $n = 10$ mice per group; * $P < 0.01$, ** $P < 0.001$.

NAE in this *in vivo* tumour model results in pathway responses and cellular phenotypic effects compatible with those observed in cultured cells.

MLN4924 inhibits tumour xenograft growth

To evaluate the anti-tumour activity of MLN4924, we administered the compound to nude mice bearing subcutaneous human tumour cell xenografts and monitored tumour growth rate. MLN4924 was administered by subcutaneous injection once (QD) or twice (BID) daily to mice bearing HCT-116 xenografts, and inhibition of tumour growth (T/C, average treated tumour volume/average control tumour volume) was calculated on the last day of treatment (Fig. 5). MLN4924 administered on a BID schedule at 30 and 60 mg kg⁻¹ inhibited tumour growth with T/C values of 0.36 and 0.15, respectively ($P < 0.001$, Fig. 5a). Significant inhibition of tumour growth was also observed when MLN4924 was administered at 30 mg kg⁻¹ (T/C = 0.49, $P < 0.001$) and 60 mg kg⁻¹ (T/C = 0.3, $P < 0.001$) on a QD schedule. Notably, a total dose of 60 mg kg⁻¹ day⁻¹ gave comparable tumour growth inhibition whether it was delivered as 60 mg kg⁻¹ QD or 30 mg kg⁻¹ BID. Less frequent administration of MLN4924 was also found to be efficacious. MLN4924 was administered at 60 mg kg⁻¹ BID on two different daily dosing schedules; either three cycles of two-days treatment followed by five treatment-free days, or two cycles of five-days treatment followed by five treatment-free days (Fig. 5b). Statistically significant inhibition of tumour growth was observed with both of these schedules (T/C = 0.36, $P < 0.001$ and T/C = 0.23, $P < 0.001$, respectively). Furthermore, MLN4924 administered once daily at 60 mg kg⁻¹ for three cycles of two-days treatment followed by five treatment-free days, resulted in modest but significant tumour growth inhibition (T/C = 0.57, $P < 0.01$). All doses and schedules were well tolerated, with an average weight loss for all dose groups at the end of treatment of less than 10% (data not shown).

The anti-tumour activity of MLN4924 was also evaluated in mice bearing H522 lung tumour xenografts (Fig. 5c). Significant tumour growth inhibition was observed after continuous daily administration of MLN4924 at 30, 60 and 90 mg kg⁻¹ BID in this model with 10/10 regressions observed at the 60 and 90 mg kg⁻¹ doses (T/C at day 14 = 0.36, 0.04 and 0.02 respectively; $P < 0.001$). The anti-tumour activity of MLN4924 in the Calu-6 lung carcinoma xenograft is described in Supplementary Fig. 6. These results demonstrate that MLN4924 treatment inhibits the growth of human tumour xenografts in mice, and is efficacious when administered on various daily and less frequent schedules.

Conclusions

Here we have described the initial characterization of MLN4924, a small molecule inhibitor of NAE that represents a new approach to targeting the UPS for the treatment of cancer. MLN4924 completely

inhibits detectable NAE pathway function in cells, disrupting the turnover of CRL substrates, with important roles in cell-cycle progression and survival. Our results indicate that inhibition of the NAE pathway disrupts cancer cell protein homeostasis more selectively than the inhibition of proteasome activity, which may contribute to useful differences in clinical efficacy and safety profiles. Sustained NAE pathway inhibition was found to result in the activation of apoptosis as a consequence of cell-cycle-dependent DNA re-replication. This phenotype was presumably a result of the inability of the cell to degrade the CRL substrate CDT1, which has been shown to induce re-replication when overexpressed. Similar cell-cycle profiles were obtained when NAE levels were reduced by RNAi or when NAE activity was compromised in a temperature-sensitive mutant cell line^{45,46}.

In vivo, we demonstrated that MLN4924 suppressed the growth of human tumour xenografts at doses and schedules that were well tolerated. Analysis of tumours from treated animals confirmed inhibition of the NEDD8 pathway, suggesting that these pharmacodynamic markers may have use in monitoring NAE inhibition in patients treated with MLN4924. These preclinical findings have supported the transition of MLN4924 into clinical development.

METHODS SUMMARY

The full Methods provides information about all experimental procedures: (1) generation of protein reagents for *in vitro* assays; (2) detailed description of *in vitro* E1-activating enzyme assays; (3) description of assay to assess bulk protein turnover in cultured cells; (4) description of cell viability assay; (5) list of antibodies used for western blot analysis of cultured cells and tumour lysates; (6) cell-cycle analysis using flow cytometry; (7) details for conducting tumour xenograft efficacy experiments in mice; (8) details for conducting pharmacodynamic studies in tumour-xenograft-bearing mice; (9) description of instrumentation used for quantification of pharmacodynamic markers; (10) description of assay to evaluate protein synthesis inhibition in cells; and (11) procedure for isolation of bone marrow from mouse femurs.

Full Methods and any associated references are available in the online version of the paper at www.nature.com/nature.

Received 10 October 2008; accepted 2 February 2009.

- Hershko, A. The ubiquitin system for protein degradation and some of its roles in the control of the cell division cycle. *Cell Death Differ.* 12, 1191–1197 (2005).
- Kane, R. C., Bross, P. F., Farrell, A. T. & Pazdur, R. VELCADE®: U.S. FDA Approval for the treatment of multiple myeloma progressing on prior therapy. *Oncologist* 8, 508–513 (2003).
- Kane, R. C. *et al.* Bortezomib for the treatment of mantle cell lymphoma. *Clin. Cancer Res.* 13, 5291–5294 (2007).
- Nalepa, G., Rolfe, M. & Harper, J. W. Drug discovery in the ubiquitin proteasome system. *Nature Rev. Drug Discov.* 5, 596–613 (2006).
- Hershko, A. & Ciechanover, A. The ubiquitin system. *Annu. Rev. Biochem.* 67, 425–479 (1998).
- Haas, A. L. & Rose, I. A. The mechanism of ubiquitin activating enzyme: A kinetic and equilibrium analysis. *J. Biol. Chem.* 257, 10329–10337 (1982).

7. Wilkinson, K. D. The discovery of ubiquitin-dependent proteolysis. *Proc. Natl Acad. Sci. USA* **102**, 15280–15282 (2005).
8. Kerscher, O., Felberbaum, R. & Hochstrasser, M. Modification of proteins by ubiquitin and ubiquitin-like proteins. *Annu. Rev. Cell Dev. Biol.* **22**, 159–180 (2006).
9. Gong, L. & Yeh, E. T. Identification of the activating and conjugating enzymes of the NEDD8 conjugation pathway. *J. Biol. Chem.* **274**, 12036–12042 (1999).
10. Pan, Z. Q., Kentsis, A., Dias, D. C., Yamoah, K. & Wu, K. NEDD8 on Cullin: building an expressway to protein destruction. *Oncogene* **23**, 1985–1997 (2004).
11. Petroski, M. D. & Deshaies, R. J. Function and regulation of cullin-RING ubiquitin ligases. *Nature Rev. Mol. Cell Biol.* **6**, 9–20 (2005).
12. Chiba, T. & Tanaka, K. Cullin-based ubiquitin ligase and its control by NEDD8 conjugation system. *Curr. Protein Pept. Sci.* **5**, 177–184 (2004).
13. Read, M. A. *et al.* Structural insights into NEDD8 activation of SCF^{TRCP}-dependent ubiquitination of I κ B α . *Mol. Cell Biol.* **20**, 2326–2333 (2000).
14. Podust, V. N. *et al.* A Nedd8 conjugation pathway is essential for proteolytic targeting of p27^{KIP1} by ubiquitination. *Proc. Natl Acad. Sci. USA* **97**, 4579–4584 (2000).
15. Duda, D. M. *et al.* Structural insights into NEDD8 activation of cullin-RING ligases: conformational control of conjugation. *Cell* **134**, 995–1006 (2008).
16. Saha, A. & Deshaies, R. J. Multimodal activation of the ubiquitin ligase SCF by NEDD8 conjugation. *Mol. Cell* **32**, 21–31 (2008).
17. Bohnsack, R. N. & Haas, A. L. Conservation in the mechanism of NEDD8 activation by the human AppBp1-Uba3 heterodimer. *J. Biol. Chem.* **278**, 26823–26830 (2003).
18. Walden, H., Podgorski, M. S. & Schulman, B. A. Insights into the ubiquitin transfer cascade from the structure of the activating enzyme for NEDD8. *Nature* **422**, 330–334 (2003).
19. Walden, H. *et al.* The structure of the APPBP1-UBA3-NEDD8-ATP complex reveals the basis for selective ubiquitin-like protein activation by an E1. *Mol. Cell* **12**, 1427–1437 (2003).
20. Bloch, A. & Coutsogeorgopoulos, C. Inhibition of protein synthesis by 5'-sulfamoyladenine. *Biochemistry* **10**, 4394–4398 (1971).
21. Rock, K. L. *et al.* Inhibitors of the proteasome block the degradation of most cell proteins and the generation of peptides presented on MHC class I molecules. *Cell* **78**, 761–771 (1994).
22. Nishitani, H. *et al.* Two E3 ubiquitin ligases, SCF-Skp2 and DDB1-Cul4 target human Cdt1 for proteolysis. *EMBO J.* **25**, 1126–1136 (2006).
23. Kondo, T. *et al.* Rapid degradation of Cdt1 upon UV-induced DNA damage is mediated by SCF^{Skp2} complex. *J. Biol. Chem.* **279**, 27315–27319 (2004).
24. Hu, J., McCall, C. M., Ohta, T. & Xiong, Y. Targeted ubiquitination of CDT1 by the DDB1-CUL4A-ROC1 ligase in response to DNA damage. *Nature Cell Biol.* **6**, 1003–1009 (2004).
25. Carrano, A. C., Eytan, E., Hershko, A. & Pagano, M. SKP2 is required for ubiquitin-mediated degradation of the CDK inhibitor p27. *Nature Cell Biol.* **1**, 193–199 (1999).
26. Kobayashi, A. *et al.* Oxidative stress sensor Keap1 functions as an adaptor for Cul3-based E3 ligase to regulate proteasomal degradation of Nrf2. *Mol. Cell Biol.* **24**, 7130–7139 (2004).
27. Nateri, A. S., Riera-Sans, L., DaCosta, C. & Behrens, A. The ubiquitin ligase SCF^{Fbw7} antagonizes apoptotic JNK signaling. *Science* **303**, 1374–1378 (2004).
28. Kamura, T. *et al.* Activation of HIF1 α ubiquitination by a reconstituted von-Hippel-Lindau (VHL) tumor suppressor complex. *Proc. Natl Acad. Sci. USA* **97**, 10430–10435 (2000).
29. Ye, X. *et al.* Recognition of phosphodegron motifs in human cyclin E by the SCF^{Fbw7} ubiquitin ligase. *J. Biol. Chem.* **279**, 50110–50119 (2004).
30. Donzelli, M. *et al.* Dual mode of degradation of Cdc25A phosphatase. *EMBO J.* **21**, 4875–4884 (2002).
31. Margottin-Goguet, F. *et al.* Prophase destruction of Emi1 by the SCF^{TRCP/Slimb} ubiquitin ligase activates the anaphase promoting complex to allow progression beyond prometaphase. *Dev. Cell* **4**, 813–826 (2003).
32. Winston, J. T. *et al.* The SCF^{TRCP}-ubiquitin ligase complex associates specifically with phosphorylated destruction motifs in I κ B α and β -catenin and stimulates I κ B α ubiquitination *in vitro*. *Genes Dev.* **13**, 270–283 (1999).
33. Machida, Y. J., Hamlin, J. L. & Dutta, A. Right place, right time and only once: replication initiation in Metazoans. *Cell* **123**, 13–24 (2005).
34. Arias, E. E. & Walter, J. C. Replication-dependent destruction of Cdt1 limits DNA replication to a single round per cell cycle in *Xenopus* egg extracts. *Genes Dev.* **19**, 114–126 (2005).
35. Li, X., Zhao, Q., Liao, R., Sun, P. & Wu, X. The SCF^{Skp2} ubiquitin ligase complex interacts with the human replication licensing factor Cdt1 and regulates Cdt1 degradation. *J. Biol. Chem.* **278**, 30854–30858 (2003).
36. Lovejoy, C. A., Lock, K., Yenamandra, A. & Cortez, D. DDB1 maintains genome integrity through regulation of Cdt1. *Mol. Cell Biol.* **26**, 7977–7990 (2006).
37. Higa, L. A., Mihaylov, I. S., Banks, D. P., Zheng, J. & Zhang, H. Radiation-mediated proteolysis of Cdt1 by CUL4-ROC1 and CSN complexes constitutes a new checkpoint. *Nature Cell Biol.* **5**, 1008–1015 (2003).
38. Saxena, S. & Dutta, A. Geminin and p53: deterrents to rereplication in human cancer cells. *Cell Cycle* **2**, 283–286 (2003).
39. Melixetian, M. *et al.* Loss of Geminin induces rereplication in the presence of functional p53. *J. Cell Biol.* **165**, 473–482 (2004).
40. Vaziri, C. *et al.* A p53-dependent checkpoint pathway prevents rereplication. *Mol. Cell* **11**, 997–1008 (2003).
41. Kim, Y. & Kipreos, E. T. Cdt1 degradation to prevent DNA rereplication: conserved and non-conserved pathways. *Cell Div.* **2**, 18–27 (2007).
42. Archambault, V., Ikui, A. E., Drapkin, B. J. & Cross, F. R. Disruption of mechanisms that prevent rereplication triggers a DNA damage response. *Mol. Cell Biol.* **25**, 6707–6721 (2005).
43. Zhu, W., Chen, Y. & Dutta, A. Rereplication by depletion of geminin is seen regardless of p53 status and activates a G2/M checkpoint. *Mol. Cell Biol.* **24**, 7140–7150 (2004).
44. Lin, J. J. & Dutta, A. ATR pathway is the primary pathway for activating G2/M checkpoint induction after re-replication. *J. Biol. Chem.* **282**, 30357–30362 (2007).
45. Handeli, S. & Weintraub, H. The ts41 mutation in Chinese hamster cells leads to successive S phases in the absence of intervening G2, M and G1. *Cell* **71**, 599–611 (1992).
46. Chen, Y., McPhie, D. L., Hirschberg, J. & Neve, R. L. The amyloid precursor protein-binding protein APP-BP1 drives the cell cycle through the S-M checkpoint and causes apoptosis in neurons. *J. Biol. Chem.* **275**, 8929–8935 (2000).

Supplementary Information is linked to the online version of the paper at www.nature.com/nature.

Acknowledgements As this project progressed through the discovery phase, many scientists made significant contributions to its success. The authors would like to thank all past contributors to the NAE project including M. H. Foley, V. Chau, T. Gladysheva and S. Sadis. We would also like to thank D. Bowman for technical help with imaging assays, J. Blank for technical help with protein turnover assays and A. Burkhardt, P. Veiby, M. Manfredi and B. Hibner for support and guidance.

Author Contributions T.A.S., P.G.S., M.A.M., A.J.B. and J.M.G. participated in the planning, initiation, data generation and analysis of biological experiments and preparation of the manuscript. C.A.C., E.J.O., S.V., G.S.W., S.C., S.P. and S.P.L. participated in the planning, initiation, design and execution of chemical synthesis. S.A., D.P.C., A.D., H.M., M.R., J.L.G., R.E.G. and T.Talreja performed chemical synthesis; U.N. performed *in vitro* cell culture experiments; T.Traore and J.Z. performed *in vivo* anti-tumour activity and pharmacodynamic experiments; J.Y., J.J.G. and M.P.T. performed pharmacodynamic analysis experiments; A.R.L. evaluated compound potencies in cell-based assays; K.E.B. and A.M. performed immunohistochemical experiments; M.D.S. performed crystallography studies. L.R.D., J.E.B., C.F.C., M.R. and J.B.B. provided oversight of the project, reviewed and edited the manuscript.

Author Information MLN4924 will be provided once a standard Materials Transfer Agreement has been executed. Reprints and permissions information is available at www.nature.com/reprints. The authors declare competing financial interests: details accompany the full-text HTML version of the paper at www.nature.com/nature. Correspondence and requests for materials should be addressed to T.A.S. (teresa.soucy@mpi.com).

METHODS

Protein reagents. Baculoviruses were generated with the Bac-to-Bac Expression System (Invitrogen) for the following proteins. His-NAE (NAE1 and His-tagged UBA3) and His-SAE (SAE1 and His-tagged UBA2) complexes were generated by co-infection of Sf9 cells. His-tagged mouse UAE (also known as Uba1), His-UBA6 and His-ATG7 were generated by single infection of Sf9 cells. Ubc12, Ubc9, Ubc2 (also known as UBE2A) were expressed as amino-terminally glutathione *S*-transferase (GST)-tagged fusion proteins in *Escherichia coli*. Use1 (UBE2Z) and ATG3 were expressed as N-terminally His-tagged proteins in *E. coli*. NEDD8, SUMO1 and ubiquitin were expressed as N-terminally Flag-tagged fusion proteins in *E. coli*. Expressed proteins were purified by affinity (Ni-NTA agarose, Qiagen) or conventional chromatography.

***In vitro* E1-activating enzyme assays.** A time-resolved fluorescence energy transfer assay format was used to measure the *in vitro* activity of NAE. The enzymatic reaction, containing 50 μ l 50 mM HEPES, pH 7.5, 0.05% BSA, 5 mM MgCl₂, 20 μ M ATP, 250 μ M glutathione, 10 nM Ubc12-GST, 75 nM NEDD8-Flag and 0.3 nM recombinant human NAE enzyme, was incubated at 24 °C for 90 min in a 384-well plate, before termination with 25 μ l of stop/detection buffer (0.1 M HEPES, pH 7.5, 0.05% Tween20, 20 mM EDTA, 410 mM KF, 0.53 nM Europium-Cryptate-labelled monoclonal Flag-M2-specific antibody (CisBio International) and 8.125 μ g ml⁻¹ PHYCOLINK allophycocyanin (XL-APC)-labelled GST-specific antibody (Prozyme)). After incubation for 2 h at 24 °C, the plate was read on the LJI Analyst HT Multi-Mode instrument using a time-resolved fluorescence method. A similar assay protocol was used to measure other E1 enzymes.

Assay of bulk protein turnover. HCT-116 cells were plated into 12-well plates at 1×10^5 cells per well and incubated overnight. The medium was exchanged with methionine-free DMEM (Invitrogen) containing 10% dialysed FBS and 50 μ Ci per well of [³⁵S]methionine, and the cells were incubated for 20 min to label proteins undergoing synthesis. The cells were then washed three times with DMEM supplemented with 2 mM methionine. Fresh medium containing 10% FBS, 2 mM methionine and the test compounds as described in Fig. 2 were then added. At the specified time points, media (50 μ l) was collected and subjected to liquid scintillation counting. At the end of the time course, remaining media was removed and the cells were solubilized by adding of 1 ml 0.2 N NaOH and the extract was subjected to liquid scintillation counting. The percentage of protein turnover at each time point was calculated as [(total acid soluble counts in supernatant)/(total acid soluble counts in supernatant + total counts in solubilized cells)] \times 100.

Cell viability assay. Cell suspensions were seeded at 3,000–8,000 cells per well in 96-well culture plates and incubated overnight at 37 °C. Compounds were added to the cells in complete growth media and incubated for 72 h at 37 °C. Cell number was quantified using the ATPlite assay (PerkinElmer).

Western blot analysis of cultured cells. HCT-116 cells grown in 6-well cell-culture dishes were treated with 0.1% DMSO (control) or MLN4924 for 24 h. Whole cell extracts were prepared and analysed by immunoblotting. For analysis of the E2-UBL thioester levels, lysates were fractionated by non-reducing SDS-PAGE and immunoblotted with polyclonal antibodies to Ubc12 (generated by Millennium), Ubc9 (AG Scientific) and Ubc10 (Boston Biochem). For analysis of other proteins, lysates were fractionated by reducing SDS-PAGE and probed with primary antibodies as follows: mouse monoclonal antibodies to CDT1 (Millennium), p27 (BD Transduction), geminin (Abcam), ubiquitin, securin/PTTG and p53 (Santa Cruz) or rabbit polyclonal antibodies to NRF2, Cyclin B1 (Santa Cruz) and GADD34 (Proteintech Group, Inc.). Rabbit monoclonal antibodies to NEDD8 and phosphorylated CHK1 (Ser317) were generated

by Millennium in collaboration with Epitomics, Inc. using Ac-KEIEIDIEPTDKVERIKERVEE-amide and Ac-VKYSS(pS)QPEPRT-amide as immunogens, respectively. Antibodies to pH3, cleaved PARP and cleaved caspase 3 were from Cell Signaling Technologies. Secondary HRP-labelled antibodies to rabbit IgG or mouse IgG (Santa Cruz) were used as appropriate. Blots were developed with ECL reagent (Amersham). For Supplementary Fig. 2, the secondary antibody was Alexa-680-labelled antibody to rabbit/mouse IgG (Molecular Probes) and the blots were imaged using the Li-Cor Odyssey Infrared Imaging system.

Cell-cycle analysis. Logarithmically growing HCT-116 cells were incubated with either MLN4924 or DMSO for the times indicated. Collected cells were fixed in 70% ethanol and stored overnight at 4 °C. Fixed cells were centrifuged to remove ethanol, and the pellets were resuspended in propidium iodide and RNase A in PBS for 1 h on ice protected from light. Cell-cycle distributions were determined using flow cytometry (FACS Calibur, Becton Dickinson) and analysed using Winlist software (Verity).

Tumour xenograft efficacy experiments. Female athymic NCR mice (Charles River Laboratories) were used in all *in vivo* studies. All animals were housed and handled in accordance with the Guide for the Care and Use of Laboratory Animals. Mice were inoculated with 2×10^6 HCT-116 cells (or 30–40 mg H522 tumour fragments) subcutaneously in the right flank, and tumour growth was monitored with caliper measurements. When the mean tumour volume reached approximately 200 mm³, animals were dosed subcutaneously with vehicle (10% cyclodextrin) or MLN4924. Inhibition of tumour growth (T/C) was calculated on the last day of treatment.

Pharmacodynamic marker analysis. Mice bearing HCT-116 tumours of 300–500 mm³ were administered a single MLN4924 dose, and at the indicated times tumours were excised and extracts prepared. The relative levels of NEDD8-cullin and NRF2 were estimated by quantitative immunoblot analysis (Li-cor Odyssey system) using Alexa680-labelled anti-IgG (Molecular Probes) as the secondary antibody. The statistical difference between the groups for NEDD8-cullin inhibition was determined using the Kruskal-Wallis test. For the analysis of CDT1 and phosphorylated CHK1 (Ser317) levels in tumour sections, formalin-fixed, paraffin-embedded tumour sections were stained with the relevant antibodies, amplified with HRP-labelled secondary antibodies and detected with the ChromoMap DAB Kit (Ventana Medical Systems). Slides were counterstained with haematoxylin. Images were captured using an Eclipse E800 microscope (Nikon Instruments) and Retiga EXi colour digital camera (QImaging) and processed using Metamorph software (Molecular Devices). CDT1 and phosphorylated CHK1 levels are expressed as a function of the DAB signal area.

Isolation of bone marrow cells from mice. For bone marrow pharmacodynamic studies, naive NCr-Nude mice (Taconic Farms) were administered MLN4924, and at the indicated times leg bones were excised. Marrow was flushed from the bones with PBS, pelleted by centrifugation and flash frozen. Thawed marrow was lysed in M-PER buffer (Pierce) with protease inhibitors. NEDD8-cullin levels were measured by immunoblot analysis.

Assay of protein synthesis. HCT-116 cells were plated into 6-well plates at 5×10^5 cells per well and incubated overnight. Fresh media containing inhibitors and 10 μ Ci per well of [³⁵S]methionine was added and the cells were incubated for 2 h to label proteins undergoing synthesis. After washing with ice-cold PBS, RIPA lysis buffer (250 μ l) was added and the cells were lysed for 30 min on ice. The lysate was transferred to Eppendorf tubes containing 500 μ l 0.5 mg ml⁻¹ BSA/5 mM EDTA, to which 200 μ l 100% (v/v) trichloroacetic acid was added. Precipitated proteins were filtered through glass microfibre discs and subjected to liquid scintillation counting.